Microelectronic Engineering 299 (2025) 112346

Contents lists available at ScienceDirect

Microelectronic Engineering

journal homepage: www.elsevier.com/locate/mee

A multi-user wearable waistband system for real-time health monitoring of respiration, ECG, and body temperature

Siyuan Wang [a,b,1], Ming Dong [c,d,1], Jiang He [a,b,1], Guancheng Wu [a,b], Xiang Li [e,f,g], Xiaojun Pan [a], Jiansheng Wu [h,**], Rongrong Bao [a,e,f,*], Caofeng Pan [a,e,f,*]

[a] Beijing Institute of Nanoenergy and Nanosystems, Chinese Academy of Sciences, Beijing 101400, PR China
[b] School of Nanoscience and Technology, University of Chinese Academy of Sciences, Beijing 100049, PR China
[c] Beijing Institute of Tracking and Telecommunications Technology, Beijing 100094, PR China
[d] Key Laboratory of Smart Earth, Beijing 100094, PR China
[e] Institute of Atomic Manufacturing, Beihang University, Beijing 100191, China
[f] International Research Institute for Multidisciplinary Science, Beihang University, Beijing 100191, China
[g] School of Physics, Beihang University, Beijing 100191, PR China
[h] State Key Laboratory of Flexible Electronics (LoFE) & Institute of Advanced Materials (IAM), School of Flexible Electronics (Future Technologies), Nanjing Tech University (NanjingTech), Nanjing 211816, China

ARTICLE INFO

Keywords:
Wearable device
Health monitoring
Respiration
ECG
Nursing home care

ABSTRACT

Wearable health monitoring systems have gained significant attention for real-time physiological signal tracking, particularly in elderly care settings where continuous, non-invasive monitoring is critical. Current systems, however, face limitations in multi-signal integration, user comfort, and practicality for long-term use. Existing approaches often rely on separate devices for measuring vital signs, leading to cumbersome setups and restricted mobility. Additionally, few solutions support simultaneous multi-user monitoring, hindering scalability in group care environments like nursing homes. In this study, we present a highly integrated waistband device that addresses these gaps by concurrently measuring respiration, electrocardiogram (ECG), and body temperature. The respiratory sensor employs a resistive pressure sensor. Its alignment with the ECG electrodes and the temperature sensor eliminates the need for auxiliary respiratory devices (e.g., masks) and enhances wearability. With the integration of a Bluetooth transmission circuit system, this real-time health monitoring system enables long-term stable testing for multiple users. A 24-h synchronized test involving 10 participants was conducted, demonstrating effective health monitoring capabilities and the potential to identify underlying health issues. This innovation provides a scalable, comfortable solution for intelligent healthcare systems, demonstrating practical value in elderly care applications.

1. Introduction

The growing global burden of population aging and chronic diseases has highlighted the critical need for continuous physiological monitoring in modern healthcare [1]. Traditional health monitoring for the elderly depends on regular hospital check-ups, a method that is not only costly and cumbersome but also risks delaying the detection of abnormal physiological signals. While conventional medical devices offer accurate measurements, their bulky size and operational complexity significantly limit practical application in daily wearable scenarios. To meet the continuous health monitoring needs of the aging population, numerous studies have developed wearable health monitoring devices that capture various physiological signals, such as respiration, heart rate, and body temperature [2–7].

Wearable respiratory sensors represent a cutting-edge health monitoring technology, with their core innovation lying in multimodal sensing mechanisms for precise respiratory signal acquisition [8,9]. The mainstream technologies primarily operate through thermal-humidity sensing and pressure sensing. Due to the temperature and humidity changes caused by exhaled breath, placing pyroelectric sensors or

* Corresponding authors at: Institute of Atomic Manufacturing, Beihang University, Beijing 100191, China.
** Corresponding author.
E-mail addresses: iamjswu@njtech.edu.cn (J. Wu), baorongrong@buaa.edu.cn (R. Bao), pancaofeng@buaa.edu.cn (C. Pan).
[1] S. Wang, M. Dong and J. He contributed equally to this work.

https://doi.org/10.1016/j.mee.2025.112346
Received 26 February 2025; Received in revised form 19 March 2025; Accepted 28 March 2025
Available online 6 April 2025
0167-9317/

humidity sensors near the mouth and nose can effectively detect breathing. However, these sensors typically need to be attached to a mask or worn directly below the nostrils, which can compromise aesthetics and comfort during daily use, making long-term monitoring challenging [10–13]. On the other hand, pressure sensors used for respiratory detection are typically attached to the chest or abdomen, making them convenient for long-term daily wear. They detect breathing signals by sensing pressure changes resulting from fluctuations in the chest and abdomen caused by diaphragm movement [14]. These pressure changes are minimal, necessitating that the sensors have high sensitivity to detect slight variations while remaining unaffected by external factors. Compared to capacitive [15–17], piezoelectric [18,19], and triboelectric [20] sensing mechanisms, resistive pressure sensors offer advantages such as high sensitivity and reduced susceptibility, which contribute to their widespread use in respiratory sensors [21–29].

Wearable electrocardiogram (ECG) sensors are designed to capture and analyze the electrical activity of the heart in real-time. These sensors are typically available in various forms, including adhesive patches, wristbands, or integrated within clothing, providing lightweight, comfortable, and user-friendly options for continuous daily wear [30]. Wearable ECG sensors enable users to monitor critical cardiac parameters such as heart rate and arrhythmias, while also offering continuous ECG data across diverse activities, including exercise and sleep. This continuous data stream is essential for the early detection of cardiovascular diseases and the facilitation of personalized health management strategies [31]. Traditional ECG systems utilize wet Ag/AgCl gel electrodes, which can lead to rashes and allergic reactions with prolonged use [32]. To ensure comfort during extended wear, considerable research has been conducted on dry electrodes [33,34]. Among these, conductive polymer polypyrrole (PPy) leather has garnered significant attention from researchers due to its excellent breathability and biocompatibility [35–37].

Wearable temperature sensors also represent a significant advancement in health monitoring technology, enabling real-time measurement and recording of human body temperature [38,39]. These sensors not only facilitate the monitoring of temperature fluctuations but also provide critical insights into bodily conditions and overall health status, particularly in the context of disease monitoring [40,41].

However, existing wearable technologies predominantly focus on single-parameter detection, demonstrating notable deficiencies in synchronized acquisition and comprehensive analysis of multiple bio-signals, which are crucial for early disease warning and holistic health assessment [42]. Existing systems for the simultaneous detection of multiple bio-signals often require the application of patches to various locations on the skin or the additional use of multiple devices such as masks and wristbands [43–45]. The dispersion of devices designed for monitoring different bio-signals across various body parts, coupled with the necessity to wear multiple components, reduces integration and significantly impacts the comfort and convenience of long-term wear [2,46]. There is an urgent need for a highly integrated device that allows for easy wear and long-term comfort while simultaneously monitoring multiple physiological signals [47]. Furthermore, most current research efforts have focused solely on individual health monitoring tests. In light of challenges such as an aging population and a shortage of healthcare resources, the development of a multi-user synchronous intelligent monitoring system has become increasingly imperative.

In this study, we designed a highly integrated waistband device capable of simultaneously measuring three critical physiological signals: respiration, ECG, and body temperature. The respiratory signal is captured using a resistive pressure sensor positioned on the abdomen. This sensor features a sensitive layer with an interconnected low-modulus porous structure, which can be rapidly fabricated using phase inversion and sacrificial templating methods. It exhibits ultra-high sensitivity (5732 kPa^{-1}) within a low-pressure range (0–500 Pa), enabling it to detect pressure changes caused by abdominal fluctuations during respiration. The positioning of the respiratory sensor aligns with that of the ECG sensor, facilitating seamless integration without the need for additional respiratory monitoring devices such as masks. The ECG electrodes are constructed from biocompatible conductive PPy-leather. Complemented by a commercial temperature sensor and a multi-module integrated circuit capable of wireless signal transmission, a multi-signal health monitoring system has been developed. This system allows for simultaneous use by multiple individuals and supports stable, long-term monitoring. It presents a viable solution for intelligent monitoring systems in nursing home settings, offering significant practical value for medical care.

2. Design and experiments

2.1. Application scenario conceptualization

The application scenario of the real-time health monitoring system is set in an intelligent nursing home, as illustrated in Fig. 1. Elderly individuals wear health monitoring waistbands that integrate temperature, respiration, and ECG sensors. Each waistband is equipped with a substation circuit board, which transmits the collected physiological data to a central station via a wireless Bluetooth module. The central station, located in the monitoring room, is managed by a qualified nurse. Upon receiving the physiological signals from the wearers, the system compares them with previously recorded data to assess the wearers' physiological status and generate alerts for any abnormal indicators. This health monitoring system enables simultaneous monitoring of multiple users by systematically collecting and uploading physiological data at set intervals, allowing for continuous real-time observation.

2.2. Fabrication of respiration sensor

In this work, a respiration sensor was developed using a resistive pressure sensor featuring a hierarchically porous structure. The sensing layer was fabricated through an integrated phase inversion and sacrificial template approach, as illustrated in Fig. 2(a). Initially, 15 wt% thermoplastic polyurethane (TPU) granules were dissolved in N, N-dimethylformamide (DMF) under continuous mechanical agitation at 70 °C for 6 h to obtain a homogeneous TPU/DMF solution. Sodium chloride (NaCl) particles were then incorporated into the solution at a 3:1 mass ratio (NaCl:TPU/DMF) and homogenized. The mixture was cast into a polytetrafluoroethylene (PTFE) mold with 1-mm-depth square cavities and leveled uniformly. Subsequent immersion in deionized water for 4 h initiated the phase inversion process, wherein TPU solidified while DMF and NaCl dissolved, creating interconnected pores through combined phase separation and template leaching [21]. The resulting porous TPU frame was thoroughly rinsed and dried, followed by saturation with silver nanowires (Ag NWs) aqueous solution via drop-casting. After drying and peeling, the conductive porous sensitive layer was obtained. Fig. 2(b) presents scanning electron microscopy (SEM) images revealing the microstructural characteristics of the porous TPU frame. The final flexible resistive pressure sensor was assembled by sandwiching the sensing layer between two nickel-coated textile electrodes adhered to nonwoven fabric substrates, as shown in Fig. 2(c). The sensitive layer is encapsulated around its perimeter using PET double-sided tape, and a pre-pressure is applied to ensure the sensor device is securely packaged. Fig. 2(d) illustrates the various components involved in the encapsulation process, from left to right: the non-woven fabric substrate with the attached Ni electrode, the non-woven fabric substrate with the attached PET tape and Ni electrode, and the 2 cm × 2 cm porous sensitive layer.

Fig. 2(e) illustrates the pressure-response characteristics of the sensor across a 0–3 kPa range, exhibiting an ultrahigh sensitivity of 5732 kPa^{-1} in the low-pressure regime (0–0.5 kPa), which is crucial for detecting subtle respiratory forces. The bottom right corner of Fig. 2(e) shows a photograph of the complete device, encapsulated with non-woven fabric, ready for testing. The device was secured to an elastic

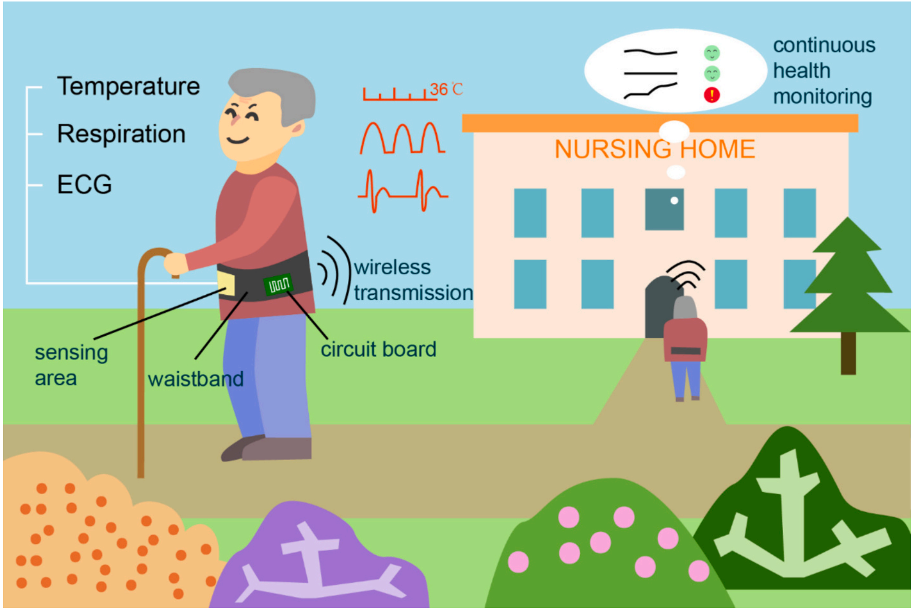

Fig. 1. Conceptual diagram of an intelligent nursing home application.

belt assembly and aligned with the abdominal region during fastening. Under cyclic breathing tests, the sensor consistently captured subtle pressure variations induced by diaphragmatic movements, demonstrating robust respiratory signal detection capability. As shown in Fig. 2 (f), real-time current response profiles delineate three consecutive breathing cycles. The pale red regions correspond to inhalation-induced current increments, while pale green regions mark exhalation-triggered current decrements, revealing distinct phases of inhalation and exhalation.

2.3. Circuit design and system integration

The circuit system consists of multiple sub-stations that wirelessly transmit data to a master station via Bluetooth technology. The master station is connected to a host computer, which displays and stores the collected data from each sub-station. A simplified electrical schematic of the sub-station is illustrated in Fig. 3(a), which includes signal detection modules for ECG, body temperature, and respiration, as well as a Bluetooth transmission module. A detailed circuit diagram can be found in Supporting Information Figure S1. The sub-station circuit is powered by a battery, making energy efficiency crucial. The battery solely powers the microcontroller unit (MCU), while the operational amplifier chip, ECG chip, and Bluetooth module are powered under the control of the MCU. The STC8A8K64D4 microcontroller is selected as the processor for the sub-station, which consumes approximately 0.4 μA in sleep mode. It utilizes an internal low-power sleep wake-up timer (consuming about 1.4 μA) to achieve periodic wake-up, facilitating long-term monitoring. The Bluetooth module chosen is the DX-BT24, which has low power consumption and minimal power supply requirements, making it suitable for battery-powered applications. This ensures prolonged continuous monitoring while worn, with a communication range of no less than 40 m in open field conditions. The 1.8 V voltage of Vref shown in Fig. 3(a) serves as the reference voltage for the analog signals generated by the ECG chip. This voltage is sent to the MCU's AVref pin as the reference voltage for analog-to-digital (A/D) conversion and is also used as a reference voltage for the respiration and body temperature detection circuits. The ECG signal acquisition module of the sub-station employs the KS1801 chip, as depicted in the lower left area of Figure S1. This chip is capable of accurately extracting weak bioelectric signals in noisy environments and performing amplification and filtering. The ECG chip KS1801 has three electrode input lines: INP (ECG+), INN (ECG-), and RLD (reference electrode). The signals from the ECG chip form a synchronous serial interface (SPI), which connects to the MCU's SPI port, allowing the MCU to control the reset and modify the gain of the ECG chip. The operational amplifier (op-amp) IC2A in the upper right corner of Figure S1 is part of the body temperature acquisition circuit. The body temperature sensor used is the commercial PT1000 sensor, which has a resistance of 1 kΩ at 0 °C, with the resistance increasing by approximately 3.9 Ω for each degree Celsius rise in temperature. This change is minimal and requires amplification by the op-amp chip for easier detection. The op-amp IC2B on the right side of Figure S1 is part of the respiration acquisition module. Due to the high initial impedance of the respiration sensor (up to approximately 5 MΩ), which does not match the input impedance of the microcontroller, the op-amp IC2B is configured as a voltage follower to achieve impedance matching. The physical layout of the sub-station circuit board is shown in Fig. 3(b), displaying the battery compartment and the connection slots for the ECG, respiration, and body temperature signals.

Fig. 3(c) illustrates the communication schematic between the sub-station and the host computer at the master station. In this experiment, Bluetooth wireless communication is utilized. The Bluetooth modules are categorized into master and slave modules, with the master module capable of initiating communication with the slave module. The slave module has its own unique address and remains in a standby state, awaiting a call. To enable simultaneous detection by multiple users, a Bluetooth slave module is installed in the master station connected to the host computer, while each sub-station circuit board is equipped with a Bluetooth master module. The Bluetooth slave module at the master station operates continuously, always ready to receive calls. When a sub-station is activated due to reaching a predetermined time, its Bluetooth master module is powered on and initiates a call to the Bluetooth slave module. The master station then enters a data passthrough mode, allowing for mutual data exchange. Upon completion of data transmission, the Bluetooth master module at the sub-station is powered down, and the Bluetooth slave module at the host computer returns to its standby state, awaiting the next call from another sub-station. This approach enables time-division multiplexing of signal transmission, ensuring synchronized detection for multiple users. The master station utilizes the DX-BT27 Bluetooth module to receive data from the sub-stations. The serial data output from the Bluetooth module is converted to USB levels and formats by the CH340E serial-to-USB converter chip, which connects to the host computer. A detailed circuit schematic

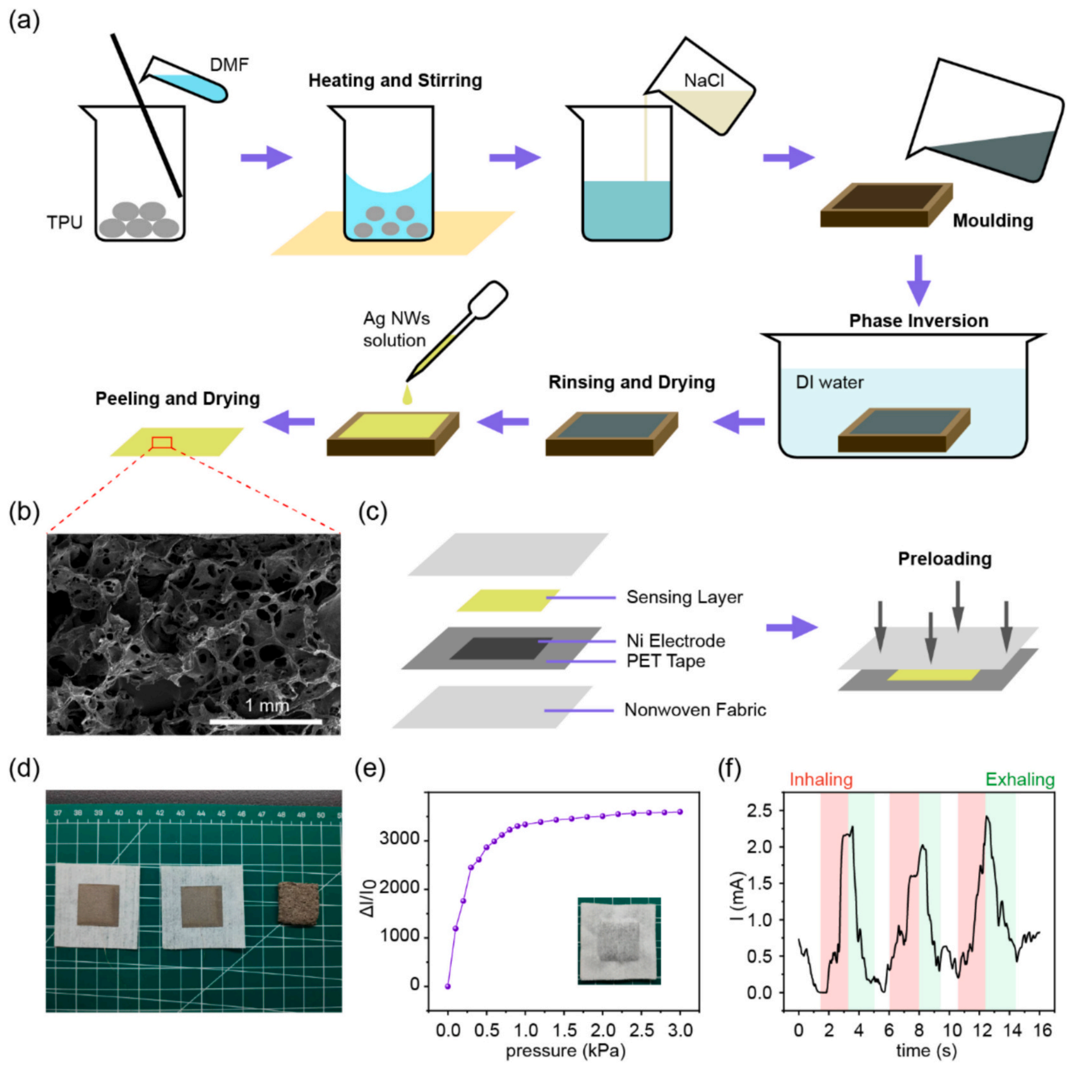

Fig. 2. Fabrication and characterization of the respiration sensor. (a) Preparation process of porous sensitive layer for pressure sensor. (b) SEM image of the porous sensitive layer. (c) Schematic diagram of the device encapsulation process. (d) Optical photographs of the various components during the encapsulation process. (e) Pressure response curve of the resistive pressure sensor. (f) Response curve of three breaths.

of the master station is provided in Supporting Information Figure S2.

Fig. 3(d) illustrates the sensor area integrated into the inner side of the waistband. The three ECG sensing electrodes are made from conductive PPy-leather to ensure comfort and breathability during wear, positioned beneath the lower ribs on either side and on the right abdomen. The central respiration sensor is encapsulated in non-woven fabric and affixed to the central abdominal area, while the commercial temperature sensor is attached to the right side of the waist. The sub-station circuit board is securely suspended on the outer side of the waistband.

Once the user has donned the waistband, the power is activated to initiate testing. The integrated health monitoring system is configured to assess physiological signals every 15 min. The testing duration of the ECG signal is set to 5 s per measurement, while the duration of the respiration signal is set to 10 s per measurement, based on the typical values of heart rate and respiratory rate. The respiratory signal changes slowly, so it is sampled at a rate of 25 points per second. In contrast, the ECG signal varies more rapidly, and is therefore sampled at 250 points per second, resulting in a total of 1250 points over a 5-s interval. Since only the waveform of the ECG signal is meaningful and the amplitude is not significant, normalization is applied to the ECG data. The ADC of the STC8A8K64D4 microcontroller is 12-bit, and the raw ECG data consists of double bytes. First, the minimum value of the 1250 ECG data points is identified, and then this minimum value is subtracted from all 1250 data points. Next, the maximum value of the adjusted 1250 data points is determined, and a normalization factor is calculated so that the maximum value multiplied by this factor equals 255. Finally, all 1250 data points are multiplied by the normalization factor. After normalization, the ECG data points are converted to single bytes, ensuring that regardless of the original data range, the normalized values will have a minimum of 0 and a maximum of 255. A similar normalization process is applied to the respiratory signal. Temperature data is collected simultaneously with each assessment.

After performing a simple normalization of the three detected physiological signals, the sub-station transmits the data wirelessly via Bluetooth to the master station's host computer, where corresponding data and waveforms are generated for subsequent health monitoring and analysis.

3. Results and discussion

3.1. 12-h single-participant testing

A continuous wear test was conducted on a single subject for a total of 12 h, from 10 AM to 10 PM. The subject's photo while wearing the waistband is shown in Fig. 4(a), where the circuit board is securely

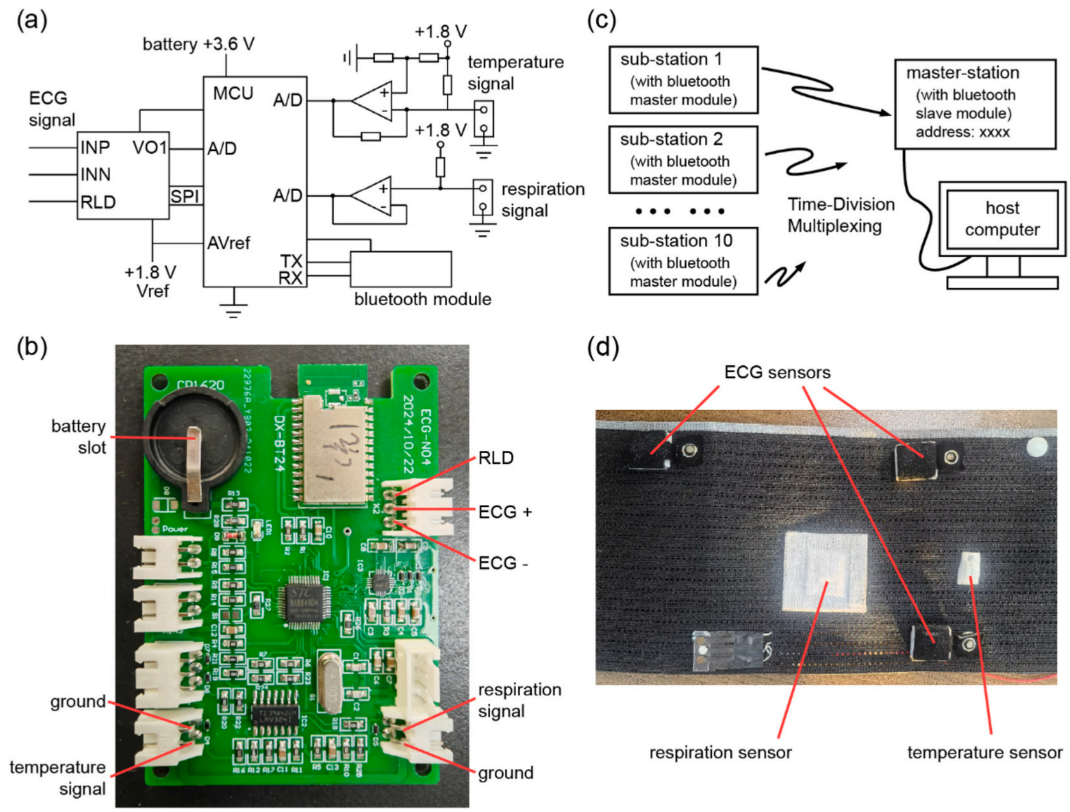

Fig. 3. Circuit design and waistband system integration. (a) Simplified circuit schematic of the sub-station, including modules for ECG, body temperature, and respiration, as well as a Bluetooth transmission module. (b) Optical image of the sub-station circuit board. (c) Diagram of communication between multiple sub-stations and the master station. (d) Optical image of the three sensors integrated into the waistband.

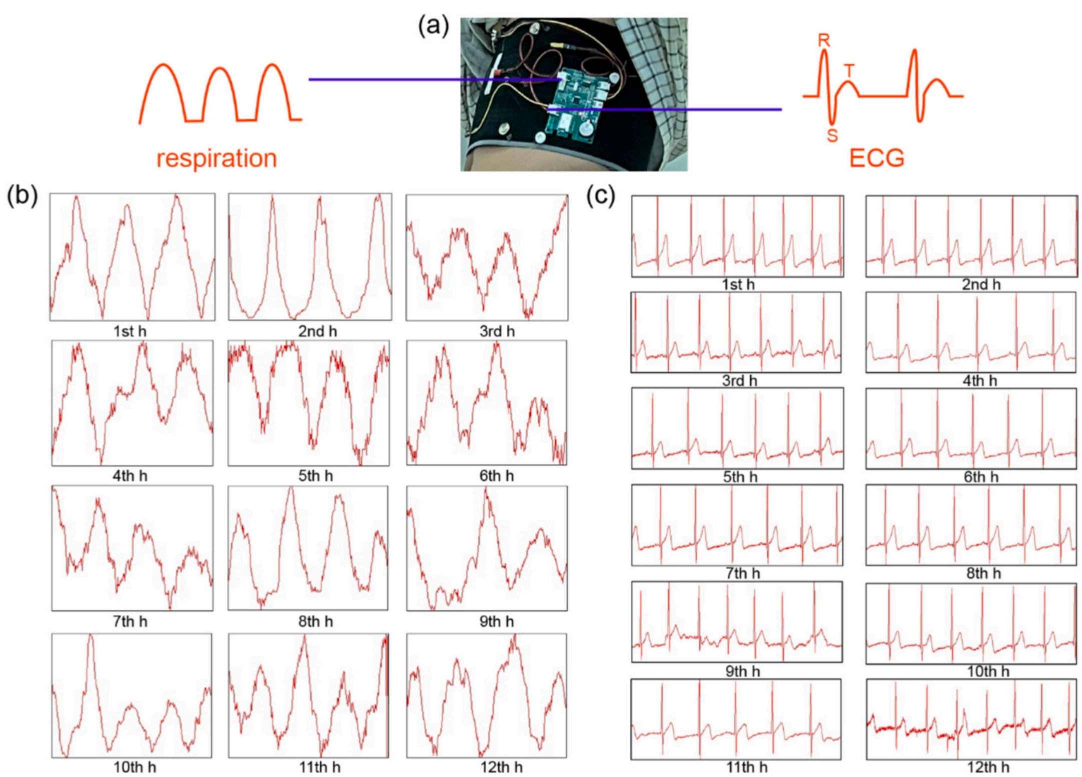

Fig. 4. Results of the 12-h single-participant testing. (a) Optical image of the subject wearing the waistband. (b) Respiratory signals over 12 h, recorded once per hour for a duration of 10 s each time. (c) ECG signals over 12 h, recorded once per hour for a duration of 5 s each time.

attached to the side of the waistband, ensuring it does not interfere with daily activities. According to the program design, the microcontroller automatically wakes up every 60 min to detect a 5-s ECG signal, a 10-s respiratory signal, and to measure body temperature. After the substation completes the data collection, it wirelessly transmits the data to the master station and then enters a low-power sleep mode, awaiting the next automatic wake-up. This allows for one physiological signal detection per hour.

Fig. 4(b) illustrates the respiratory detection signal recorded every hour during the 12-h continuous monitoring. Notable pressure changes caused by abdominal movements associated with breathing can be clearly observed. Since the respiratory signal has been normalized, the amplitude of the respiratory peaks is not significant; only the periodic changes of peaks are considered. Within the 10-s respiratory detection interval, there are typically 3 to 4 respiratory peaks, corresponding to a respiratory rate of approximately 18–24 breaths per minute, which aligns with the resting respiratory rate of adults. Fig. 4(c) presents the ECG detection signal recorded every hour during the 12-h monitoring period. The ECG signal has also been normalized, enhancing the visibility of the peaks. The electrocardiogram obtained using conductive PPy-leather as electrodes closely matches that of medical tests, with distinct characteristic peaks (R, S, and T waves) observable in each ECG signal. Within the 5-s ECG detection interval, the R peaks typically appear 5 to 7 times, corresponding to a heart rate ranging from 60 to 84 bpm, which aligns with the resting heart rate of adults.

Moreover, by combining the respiration and ECG signals, we can observe the coordinated changes between breathing and heartbeats to some extent. For instance, during the 4th to 6th hours (1 PM to 3 PM), when the subject was taking a nap, a smoother respiratory rate and a slower heart rate were noted. In the 5th hour (2 PM), both the respiratory rate and heart rate increased synchronously, reflecting the physiological relationship between breathing and heartbeat. This synchronous increase may indicate that the subject was in the rapid eye movement (REM) sleep phase, which is typically associated with vivid dreaming. In the 10th hour (7 PM), after having dinner and engaging in light activity, the respiratory rate increased slightly, and the heart rate correspondingly rose.

The variations in respiration rate and heart rate observed in this experiment can provide insights into the individual's health status. For example, heart rate variability (HRV) and changes in respiratory rate can be used to assess cardiovascular health, stress levels, and overall physiological condition, demonstrating practical value for medical health monitoring. After 12 h of continuous wear testing, the subject reported no discomfort from wearing the device, and the battery on the waistband remained sufficiently charged. The supplementary battery life experiment is presented in Supporting Information Figure S3. Utilizing the LIR1632 button cell battery from the experiment, tests were conducted at four times the normal usage intensity. The voltage remained stable over a duration of 79 h, demonstrating that this low-power system is capable of continuous operation for up to 10 days. This indicates that the health monitoring system possesses advantages of low power consumption, high stability, and high comfort, showing potential for long-term reliable wearable health monitoring.

3.2. 24-h multi-participant synchronous testing

Following the 12-h continuous testing on a single subject, we conducted a 24-h synchronous wear test with 10 participants to validate the feasibility of this system in a multi-person nursing home setting. After ten participants (A-J) donned their waistbands, we sequentially powered on each participant's system at one-minute intervals. The first test for participant A began at 10:01 AM, followed by participant B at 10:02 AM, and so on, until participant J was tested at 10:10 AM. During each participant's testing period, the substation system collected data and wirelessly transmitted it to the master station, while simultaneously synchronizing with the master station to adjust the sub-station timer for accurate timing. This way, the master station's computer received signals from specific participants at fixed intervals, allowing the data to be organized into individual health monitoring profiles based on the time of receipt, thus achieving synchronous testing for multiple participants. After data transmission was complete, the substation entered a sleep mode and would automatically wake up at the designated time for the next round of testing. In this experiment, the testing interval was set to one hour; however, if more frequent monitoring is required, it can be adjusted to complete a round of testing for all participants every 15 min.

Participants were free to move around the room. Starting from 10:00 AM on the first day, physiological signals were automatically collected every hour until 9:10 AM the following day, completing the 24-h synchronous health monitoring for all ten participants. The processed data for participants A-J revealed variations in their respiratory rates (as shown in Fig. 5(a)), heart rates (Fig. 5(b)), and body temperatures (Fig. 5(c)). The comparative analysis among participants highlighted significant individual differences in physiological signals. For instance, participant C exhibited a consistently elevated heart rate within the normal range (60–100 bpm), while participant D displayed signs of sinus bradycardia. Some participants showed higher surface temperatures, whereas others maintained lower body temperatures. The trends in physiological signal variations also reflected the participants' physiological states. For example, participants generally exhibited higher heart rates during the day when awake and lower heart rates at night when asleep, consistent with typical human patterns. The interplay and abnormal changes among the three physiological signals—respiration, heart rate, and body temperature—could also indicate potential health risks for the participants, such as increased respiration, elevated heart rate, and abnormal temperature due to infections.

Furthermore, during this testing, subject I exhibited premature ventricular contractions, which were captured before bedtime. The waveform of the premature beat is illustrated in Fig. 5(d). Additionally, irregularities in heart rhythm were observed in subject E, as shown in the electrocardiogram presented in Supporting Information Figure S4. This indicates that the system is capable of continuous monitoring of physiological signals and can detect potential health issues, providing valuable guidance and support for medical care.

Fig. 5(e) displays the respiratory and ECG signals obtained from a participant during vigorous exercise, showing a clear increase in both respiratory rate (27 bpm) and heart rate (132 bpm). The signal waveforms remained distinctly recognizable even during intense physical activity. The baseline of the ECG signal may drift due to changes in the contact between the electrodes and the skin caused by body movement. Additionally, sweat from exercise may also affect the baseline of the ECG signal to some extent. However, the R-R interval used to determine heart rate remains unaffected. This demonstrates that the waistband monitoring device functions effectively during exercise, making it suitable for long-term wear and monitoring.

4. Conclusion

In this study, we envisioned a smart nursing home as the application scenario and designed a real-time health monitoring system capable of conducting synchronous assessments for multiple participants. Subjects can achieve long-term automatic monitoring of three physiological signals—respiration, ECG, and body temperature—simply by wearing a highly integrated waistband. The device is comfortable to wear throughout the monitoring period, and is allowed for free movement without significant discomfort.

Initially, we conducted a 12-h continuous test with a single participant to validate the stability and reliability of the health monitoring system. Subsequently, we organized a synchronous health monitoring experiment involving ten participants over a 24-h period, which provided clear insights into the physiological signal variations of each individual. These variations were found to be consistent with observed physiological activities of the subjects, such as exercise and sleep. This

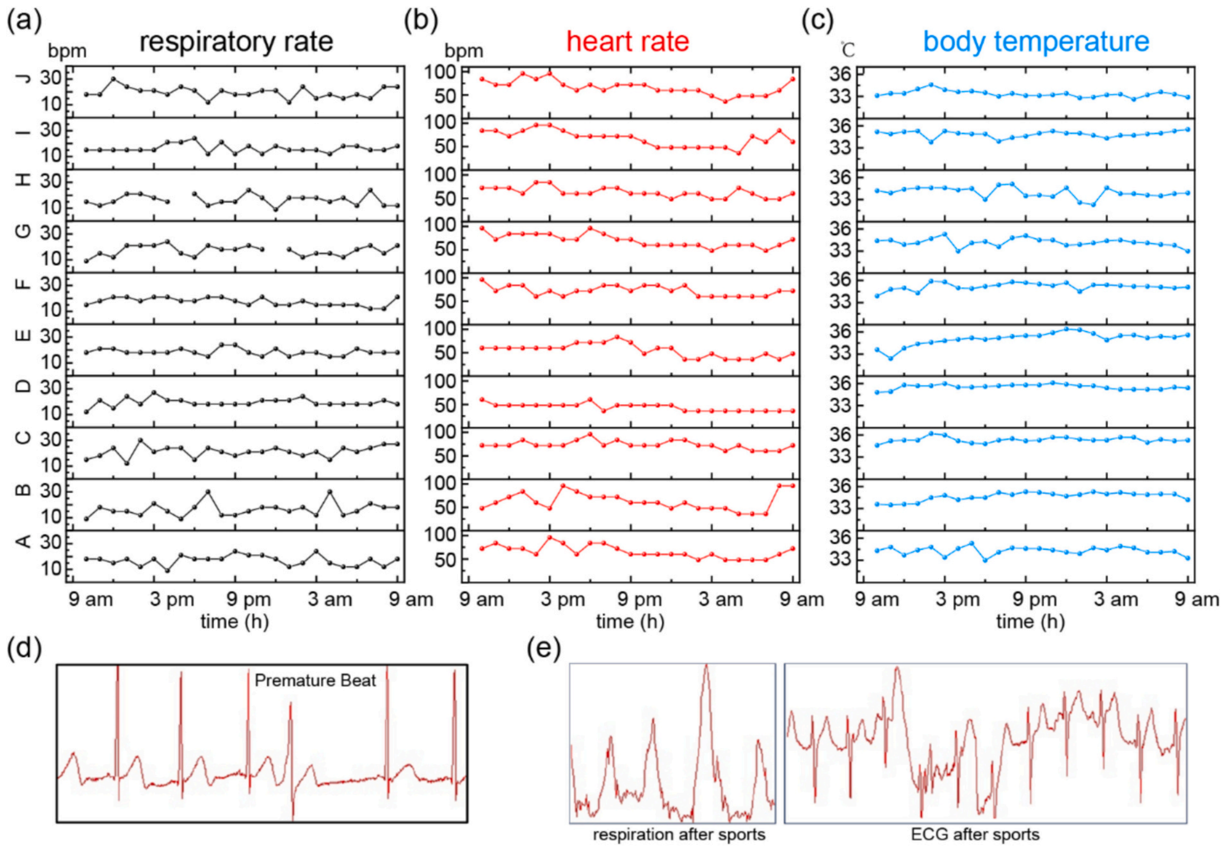

Fig. 5. Results of the 24-h multi-participant synchronous testing. (a) Trend chart of respiratory rate variations for ten subjects A-J over 24 h. (b) Trend chart of heart rate variations for ten subjects A-J over 24 h. (c) Trend chart of body temperature variations for ten subjects A-J over 24 h. (d) Observation of premature ventricular contractions in subject I during the 24-h monitoring. (e) Respiratory and ECG signals detected in a subject during intense exercise.

indicates that the system is capable of long-term monitoring of the lifestyle habits and physiological indicators of the elderly population. Additionally, the experiment revealed physiological phenomena such as premature ventricular contractions and sinus bradycardia, demonstrating the system's potential to identify underlying health issues. In summary, our work successfully achieved long-term real-time monitoring of multiple participants across various physiological indicators, offering a practical solution for future intelligent healthcare systems.

Supplementary data to this article can be found online at https://doi.org/10.1016/j.mee.2025.112346.

Declaration of competing interest

The authors declare no conflict of interest.

Acknowledgements

S. Wang, M. Dong and J. He contributed equally to this work. The authors thank the support of National Natural Science Foundation of China (No. 52371202, 52192610, 62422120), Natural Science Foundation of Beijing (L223006), and the National Key R&D Program of China (2021YFB3200302 and 2021YFB3200304).

Data availability

The data that support the findings of this study are available from the corresponding author upon reasonable request.

References

[1] C. Chen, S. Ding, J. Wang, Nat. Med. 29 (7) (2023) 1623–1630, https://doi.org/10.1038/s41591-023-02391-8.
[2] K. Mahato, T. Saha, S. Ding, S.S. Sandhu, A.-Y. Chang, J. Wang, Nat. Electron. 7 (9) (2024) 735–750, https://doi.org/10.1038/s41928-024-01247-4.
[3] J. Kim, A.S. Campbell, B.E. de Avila, J. Wang, Nat. Biotechnol. 37 (4) (2019) 389–406, https://doi.org/10.1038/s41587-019-0045-y.
[4] Z. Chen, Q. Hua, G. Shen, J. Semicond. 45 (2024) 8, https://doi.org/10.1088/1674-4926/24050042.
[5] Y. Shi, Z. Zhang, Q. Huang, Y. Lin, Z. Zheng, J. Semicond. 44 (2023) 2, https://doi.org/10.1088/1674-4926/44/2/021601.
[6] Q. Hua, G. Shen, J. Semicond. 44 (2023) 10, https://doi.org/10.1088/1674-4926/44/10/100401.
[7] J. Tao, M. Dong, L. Li, C. Wang, J. Li, Y. Liu, et al., Microsyst. Nanoeng. 6 (2020) 62, https://doi.org/10.1038/s41378-020-0171-1.
[8] S. Shen, Q. Zhou, G. Chen, Y. Fang, O. Kurilova, Z. Liu, et al., Mater. Today 72 (2024) 140–162, https://doi.org/10.1016/j.mattod.2023.12.003.
[9] X. Li, G. Wu, C. Pan, R. Bao, J. Semicond. 46 (2025) 1, https://doi.org/10.1088/1674-4926/24090044.
[10] H. Xue, Q. Yang, D. Wang, W. Luo, W. Wang, M. Lin, et al., Nano Energy 38 (2017) 147–154, https://doi.org/10.1016/j.nanoen.2017.05.056.
[11] J. He, R. Wei, X. Ma, W. Wu, X. Pan, J. Sun, et al., Adv. Mater. 36 (25) (2024) e2401931, https://doi.org/10.1002/adma.202401931.
[12] X. Chen, L. Kong, J.A. Mehrez, C. Fan, W. Quan, Y. Zhang, et al., Nano Lett. 15 (1) (2023) 149, https://doi.org/10.1007/s40820-023-01107-4.
[13] Z. Zhen, Z. Li, X. Zhao, Y. Zhong, L. Zhang, Q. Chen, et al., Small 14 (15) (2018) e1703848, https://doi.org/10.1002/smll.201703848.
[14] G. Chen, X. Zhao, S. Andalib, J. Xu, Y. Zhou, T. Tat, et al., Matter 4 (11) (2021) 3725–3740, https://doi.org/10.1016/j.matt.2021.09.012.
[15] S. Sharma, A. Chhetry, M. Sharifuzzaman, H. Yoon, J.Y. Park, ACS Appl. Mater. Interfaces 12 (19) (2020) 22212–22224, https://doi.org/10.1021/acsami.0c05819.
[16] R. Han, Y. Liu, Y. Mo, H. Xu, Z. Yang, R. Bao, et al., Adv. Funct. Mater. 33 (2023) 51, https://doi.org/10.1002/adfm.202305531.
[17] R. Bao, J. Tao, J. Zhao, M. Dong, J. Li, C. Pan, Sci. Bull. (Beijing) 68 (10) (2023) 1027–1037, https://doi.org/10.1016/j.scib.2023.04.019.
[18] Y. Su, W. Li, X. Cheng, Y. Zhou, S. Yang, X. Zhang, et al., Nat. Commun. 13 (1) (2022) 4867, https://doi.org/10.1038/s41467-022-32518-3.

[19] Y. Su, C. Chen, H. Pan, Y. Yang, G. Chen, X. Zhao, et al., Adv. Funct. Mater. 31 (2021) 19, https://doi.org/10.1002/adfm.202010962.

[20] H.-J. Qiu, W.-Z. Song, X.-X. Wang, J. Zhang, Z. Fan, M. Yu, et al., Nano Energy 58 (2019) 536–542, https://doi.org/10.1016/j.nanoen.2019.01.069.

[21] Y. Liu, J. Tao, Y. Mo, R. Bao, C. Pan, Adv. Mater. 36 (21) (2024) e2313857, https://doi.org/10.1002/adma.202313857.

[22] H. Pan, G. Chen, Y. Chen, A. Di Carlo, M.A. Mayer, S. Shen, et al., Biosens. Bioelectron. 222 (2023) 114999, https://doi.org/10.1016/j.bios.2022.114999.

[23] J. He, S.Y. Wang, R.H. Han, Y. Liu, W.C. Gao, R.R. Bao, et al., Adv. Funct. Mater. (2024) 2418791, https://doi.org/10.1002/adfm.202418791.

[24] Y. Liu, J. Tao, W. Yang, Y. Zhang, J. Li, H. Xie, et al., Small 18 (8) (2022) e2106906, https://doi.org/10.1002/smll.202106906.

[25] Z. Dai, M. Wang, Y. Wang, Z. Yu, Y. Li, W. Qin, et al., J. Semicond. 46 (2025) 1, https://doi.org/10.1088/1674-4926/24080027.

[26] Y. Liu, H. Xu, M. Dong, R. Han, J. Tao, R. Bao, et al., Adv. Mater. Technol. 7 (2022) 12, https://doi.org/10.1002/admt.202200504.

[27] X. Pan, J. Li, Z. Xu, Y. Liu, W. Gao, R. Bao, et al., Mater. Today Phys. 48 (2024) 101562, https://doi.org/10.1016/j.mtphys.2024.101562.

[28] G. Wu, X. Li, R. Bao, C. Pan, Adv. Funct. Mater. 34 (2024) 44, https://doi.org/10.1002/adfm.202405722.

[29] X. Li, Y. Lin, L. Cui, C. Li, Z. Yang, S. Zhao, et al., ACS Appl. Mater. Interfaces 15 (48) (2023) 56233–56241, https://doi.org/10.1021/acsami.3c11760.

[30] S. Ramasamy, A. Balan, Sens. Rev. 38 (4) (2018) 412–419, https://doi.org/10.1108/sr-06-2017-0110.

[31] F. Yin, J. Chen, H. Xue, K. Kang, C. Lu, X. Chen, et al., J. Semicond. 46 (2025) 1, https://doi.org/10.1088/1674-4926/24080026.

[32] A. Searle, L. Kirkup, Physiol. Meas. 21 (2) (2000) 271–283, https://doi.org/10.1088/0967-3334/21/2/307.

[33] J.-Y. Baek, J.-H. An, J.-M. Choi, K.-S. Park, S.-H. Lee, Sensors Actuators A Phys. 143 (2) (2008) 423–429, https://doi.org/10.1016/j.sna.2007.11.019.

[34] G. Kumar, B. Duggal, J.P. Singh, Y. Shrivastava, J. Biomed. Mater. Res. A 113 (1) (2025) e37845, https://doi.org/10.1002/jbm.a.37845.

[35] K. Zhang, N. Kang, B. Zhang, R. Xie, J. Zhu, B. Zou, et al., Adv. Electron. Mater. 6 (8) (2020) 2000259, https://doi.org/10.1002/aelm.202000259.

[36] Y. Song, Y. Huang, Y. Zou, L. Gou, J. Mater. Sci. Mater. Electron. 32 (4) (2021) 4891–4902, https://doi.org/10.1007/s10854-020-05229-y.

[37] Y. Zhao, R. Zhang, Y. Liu, F. Wang, S. Hu, F. Yang, et al., Sensors Actuators A Phys. (2025) 382, https://doi.org/10.1016/j.sna.2024.116145.

[38] B.A. Kuzubasoglu, E. Sayar, C. Cochrane, V. Koncar, S.K. Bahadir, J. Mater. Sci. Mater. Electron. 32 (4) (2021) 4784–4797, https://doi.org/10.1007/s10854-020-05217-2.

[39] J. Shin, B. Jeong, J. Kim, V.B. Nam, Y. Yoon, J. Jung, et al., Adv. Mater. 32 (2) (2020) e1905527, https://doi.org/10.1002/adma.201905527.

[40] Q. Li, L.N. Zhang, X.M. Tao, X. Ding, Adv. Healthc. Mater. 6 (2017) 12, https://doi.org/10.1002/adhm.201601371.

[41] Z. Yang, H. Song, H. Ding, J. Semicond. 46 (2025) 1, https://doi.org/10.1088/1674-4926/24100003.

[42] H.C. Ates, P.Q. Nguyen, L. Gonzalez-Macia, E. Morales-Narvaez, F. Guder, J. J. Collins, et al., Nat. Rev. Mater. 7 (11) (2022) 887–907, https://doi.org/10.1038/s41578-022-00460-x.

[43] H.U. Chung, A.Y. Rwei, A. Hourlier-Fargette, S. Xu, K. Lee, E.C. Dunne, et al., Nat. Med. 26 (3) (2020) 418–429, https://doi.org/10.1038/s41591-020-0792-9.

[44] H.U. Chung, B.H. Kim, J.Y. Lee, J. Lee, Z. Xie, E.M. Ibler, et al., Science 363 (2019) 6430, https://doi.org/10.1126/science.aau0780.

[45] J. Zhong, Z. Li, M. Takakuwa, D. Inoue, D. Hashizume, Z. Jiang, et al., Adv. Mater. 34 (6) (2022) e2107758, https://doi.org/10.1002/adma.202107758.

[46] T. Stuart, J. Hanna, P. Gutruf, APL Bioeng. 6 (2) (2022) 021502, https://doi.org/10.1063/5.0086935.

[47] Q. Hua, J. Sun, H. Liu, R. Bao, R. Yu, J. Zhai, et al., Nat. Commun. 9 (1) (2018) 244, https://doi.org/10.1038/s41467-017-02685-9.